

Holographic Superfluids and the Dynamics of Symmetry Breaking

M. J. Bhaseen,¹ J. P. Gauntlett,² B. D. Simons,¹ J. Sonner,³ and T. Wiseman²

¹*Cavendish Laboratory, University of Cambridge, Cambridge, CB3 0HE, U.K.*

²*Blackett Laboratory, Imperial College, London SW7 2AZ, U.K.*

³*DAMTP, University of Cambridge, CB3 0WA, U.K.*

(Dated: May 18, 2022)

We explore the far from equilibrium response of a holographic superfluid using the AdS/CFT correspondence. We establish the dynamical phase diagram corresponding to quantum quenches of the order parameter source field. We find three distinct regimes of behaviour that are related to the spectrum of black hole quasi-normal modes. These correspond to damped oscillations of the order parameter, and over-damped approaches to the superfluid and normal states. The presence of three regimes, which includes an emergent dynamical temperature scale, is argued to be a generic feature of time-reversal invariant systems that display continuous symmetry breaking.

PACS numbers: 74.40.Gh, 11.25.Tq

In the last few years there has been a wealth of experimental activity exploring the non-equilibrium properties of quantum many body systems. Recent advances include observations of long-lived oscillations in colliding one-dimensional (1D) Bose gases [1], and the dynamics of cold atoms following a quantum quench [2, 3]. Non-equilibrium measurements have also been exploited to reveal the amplitude mode in 2D superfluids [4], and to explore pairing in high temperature superconductors [5]. In parallel there has also been significant theoretical work on strongly correlated systems, particularly in 1D, where analytical and numerical progress is possible. This includes predictions for the time dependence following a quench to a quantum critical point [6], and the development of numerical techniques [7–9]. Significant progress has also been made on the quench dynamics of integrable models, including the Ising model, the 1D Bose gas, and the BCS Hamiltonian; for a recent review see Ref. [10].

A notable feature of the integrable dynamics of the BCS Hamiltonian, following an abrupt change in the pairing interactions, is a regime of undamped persistent oscillations of the order parameter [11–13]; see also Refs. [14, 15]. This is accompanied by a transition to a regime of damped collective oscillations as the strength of the quench is increased [16]. These results have been obtained using time-dependent generalisations of the BCS wave function and through exact spectral considerations. They are expected to hold in the collisionless regime, for timescales shorter than the energy relaxation time [17, 18]. In spite of these achievements, it is challenging to see how such results are modified at late times in the collision dominated regime. In particular, do the oscillations and the transition withstand quantum and thermal fluctuations and departures from integrability? Indeed, related considerations apply to other integrable systems, and generalizing non-equilibrium results to more generic situations, including higher dimensions, is a major open challenge.

In this respect, the AdS/CFT correspondence [19–21]

can offer valuable insights. It recasts certain strongly interacting quantum systems, which are large N field theories, in terms of weakly coupled gravitational models in at least one dimension higher. This provides access to the quantum response functions from the classical solutions of the corresponding gravitational equations. Moreover, finite temperatures can be incorporated by the inclusion of black hole solutions. This real time gravitational approach therefore avoids the analytical continuation required by the imaginary time path integral. It is thus ideally suited to non-equilibrium problems at finite temperature and in arbitrary dimension [22–27]. The methods are very powerful when combined with numerical solution of the equations of motion, as they allow access to the far from equilibrium response over the entire time evolution [28–33].

In this manuscript we will focus on the far from equilibrium response of a holographic superfluid [29, 34, 35] under a spatially homogeneous and isotropic quench. Our primary aim is to reveal the presence of three regimes of non-equilibrium response, including a dynamical transition from under-damped to over-damped collective oscillations. This transition occurs within the superfluid phase, and we argue that this transition will feature in other (holographic and non-holographic) time-reversal invariant systems that display continuous symmetry breaking.

Model.— We consider the original action for a holographic superfluid, describing a complex scalar field ψ , with charge q and mass m , minimally coupled to electromagnetism and gravity in 3+1 dimensions [34, 35]:

$$S = \frac{1}{2\kappa^2} \int d^4x \sqrt{-g} \left[R + \frac{6}{\ell^2} - \frac{F^2}{4} - |D\psi|^2 - m^2 |\psi|^2 \right], \quad (1)$$

where $F_{ab} = \partial_a A_b - \partial_b A_a$, $D_a = \partial_a - iqA_a$, and the radius ℓ parameterizes the inverse curvature of AdS space-time. The model is dual to a strongly coupled large N CFT in 2+1 dimensions, residing on the AdS boundary; for recent reviews see Refs. [36, 37]. This CFT is time-reversal

invariant and has a global U(1) symmetry whose conserved current, J_μ , is dual to A_a . Likewise, the field ψ is dual to an operator \mathcal{O} in the CFT with scaling dimension Δ fixed by m . For simplicity, we choose $q = 2$ and $m^2 = -2/\ell^2$ with $\Delta = 2$. As we will discuss more fully below, the operator \mathcal{O} corresponds to a superfluid order parameter for the boundary theory [34, 35]. In the remainder we will denote $1/(2\kappa^2) \equiv \mathcal{C}/\ell^2$ and choose units with $\ell = 1$. Here, \mathcal{C} is a measure of the number of local degrees of freedom in the CFT, going as $\mathcal{C} \sim N^{3/2}$ at large N . As we will see below, the model exhibits global U(1) symmetry breaking, which is possible in the 2+1 D CFT due to large N [35]. We emphasise that other holographic superfluid models, including 3+1 D CFTs, will exhibit analogous phenomena.

In order to investigate the dynamics of the model we need to specify the space-time coordinates and the metric. Assuming spatial homogeneity and isotropy of the CFT under time evolution, the most general metric is

$$ds^2 = z^{-2} [-F dt^2 - 2 dt dz + S^2(dx_1^2 + dx_2^2)], \quad (2)$$

where (t, x_1, x_2) are common to both the boundary and bulk theories, and the coordinate z specifies the additional direction in the bulk space-time. This corresponds to ingoing Eddington–Finkelstein coordinates, where the asymptotic AdS boundary is located at $z = 0$; see Fig. 1. Here $F(t, z)$ and $S(t, z)$ depend only on t and z . Likewise $\psi = \psi(t, z)$ and $A_t = A_t(t, z)$, where the spatial components of A_a are set to zero. We may thus examine the dynamics as a function of t and z alone; see Fig. 1.

First, let us recall that in equilibrium, the CFT at finite temperature and charge density is described by an electrically charged static black hole whose properties are independent of t . The high temperature unbroken phase of the equilibrium CFT is described by an AdS-Reissner–Nordström (AdS-RN) black hole [34, 35] with

$$F = 1 - 2Mz^3 + (\rho^2/4)z^4, \quad S = 1, \quad A_t = \mu - \rho z, \quad (3)$$

and $\psi = 0$. Here μ and ρ are the chemical potential and the charge density of the dual CFT; the latter is related to the expectation value of the current density operator via the relation $\langle J_t \rangle \equiv \rho/2\kappa^2$. Likewise, the mass M is proportional to the energy density of the CFT. Similarly, the Hawking temperature, $T_H(\rho, M)$, corresponds to the temperature T of the CFT. At $T_c \approx 0.090\mu$ the AdS-RN black hole becomes unstable and the CFT is described by a new family of black hole solutions with $\psi \neq 0$ [35]. Asymptotically close to the AdS boundary ψ has the coordinate expansion $\psi = z\psi_1 + z^2\psi_2 + \dots$ with $\psi_1 = 0$. Analogous to the identifications following Eq. (3), the AdS/CFT correspondence allows one to identify ψ_1 as a source for the superfluid order parameter in the dual CFT, and ψ_2 as the expectation value, $\langle \mathcal{O} \rangle \equiv \psi_2/2\kappa^2$. Hence, these black holes with $\psi \neq 0$ describe a superfluid phase in which the global U(1) symmetry is spontaneously broken.

Gaussian Quantum Quench.—We now analyse the far from equilibrium dynamics of the dual CFT, at finite temperature and charge density, by numerically constructing time-dependent black hole solutions, where F, S, A_t, ψ depend on both z and t . Near the AdS boundary at $z = 0$ the latter have the asymptotic expansion

$$\psi = z\psi_1(t) + z^2\psi_2(t) + \dots, \quad A_t = \mu(t) - z\rho(t) + \dots \quad (4)$$

The holographic renormalization group allows one to establish the time-dependent correspondence

$$\langle J_t(t) \rangle = \frac{\rho(t) - \dot{\mu}(t)}{2\kappa^2}, \quad \langle \mathcal{O}(t) \rangle = \frac{[\psi_2(t) + 2i\mu(t)\psi_1(t)]}{2\kappa^2}, \quad (5)$$

in our space-time coordinates and gauge. We take as our initial state a superfluid corresponding to a black hole with $\psi \neq 0$ [35]. We set the initial temperature to $T_i = 0.5T_c$ for numerical convenience; as we will see, similar results are also expected for other values of T_i . We then apply a quench of the source field $\psi_1(t)$, conjugate to $\langle \mathcal{O}(t) \rangle$. Specifically, we apply a Gaussian-type quench, centred on $t = 0$, by imposing

$$\psi_1(t) = \bar{\delta} e^{-(t/\bar{\tau})^2}, \quad (6)$$

where $\bar{\delta}$ and $\bar{\tau}$ characterise the quench strength and time-scale respectively. The chemical potential of the initial state, μ_i , sets the scale for the resulting dynamics and we use it to define dimensionless $\delta \equiv \bar{\delta}/\mu_i$ and $\tau \equiv \mu_i\bar{\tau}$. For definiteness, we set $\tau = 0.5$ and will vary δ . We track the dynamics by solving the equations of motion of (1) numerically. As discussed in the Supplementary Material we choose a gauge for $\mu(t)$ which keeps the initial and final charge densities the same while the quench injects energy into the system. Then $\mu(t)$ interpolates from the initial value, μ_i , to a final chemical potential, μ_f . We find similar results for other values of τ , and also for quenches which do not preserve the equality of initial and final charge density. As we shall see later, our quench is abrupt compared with the emergent relaxation time-scale. Further details on solving the equations of motion, which are non-linear PDEs in t, z , are provided in the Supplementary Material. Here we focus on the main results, summarised in Figs 1-3.

Dynamical Phase Diagram.—In Fig. 2 we show the dynamical phase diagram as a function of the quench strength, δ . It displays three regimes of late-time behaviour whose asymptotics are governed by the gauge-invariant equation

$$|\langle \mathcal{O}(t) \rangle| \simeq |\langle \mathcal{O} \rangle_f + \mathcal{A}e^{-i\omega t}|, \quad (7)$$

where $\langle \mathcal{O} \rangle_f$ is the final order parameter, \mathcal{A} is an amplitude pre-factor, and ω is a complex frequency in the lower half-plane. In region III it displays exponential decay towards a vanishing final order parameter $|\langle \mathcal{O} \rangle_f| = 0$, so

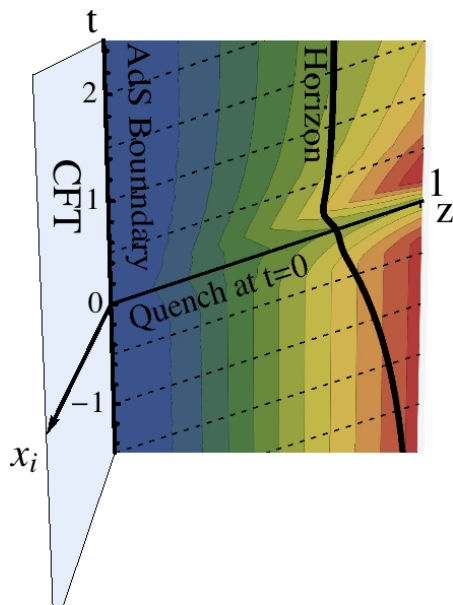


FIG. 1. Schematic representation of the space-time coordinates (2). We show data for the time evolution of the real part of the scalar field $\psi(t, z)$ following a Gaussian quench at $t = 0$ with $\delta = 0.15$, from a superfluid black hole initial state as $t \rightarrow -\infty$ with $T_i/T_c = 0.5$. The behaviour near the AdS boundary at $z = 0$ is used to extract the dynamics of the superfluid order parameter $\langle \mathcal{O}(t) \rangle$ shown in Figs 2,3.

that for large quench strengths we exit the initial superfluid phase completely. In contrast, in region II it exhibits non-oscillatory exponential decay with $\text{Re}(\omega) = 0$ towards $|\langle \mathcal{O} \rangle_f| \neq 0$. As we shall see later, this corresponds to the presence of a gapped “amplitude” mode and a gapless “phase” mode in the superfluid phase. However, in region I it exhibits exponentially damped oscillations with $\text{Re}(\omega) \neq 0$ towards $|\langle \mathcal{O} \rangle_f| \neq 0$, so that for smaller quench strengths there is another regime of dynamics. For the parameters used in Fig. 2, the transition from I to II occurs at a critical quench strength $\delta_* \approx 0.14$, whilst the transition from II to III occurs at $\delta_c \approx 0.21$.

The behaviour shown in Fig. 2 is reminiscent of the dynamical phase diagram for a BCS superconductor [16], despite the fact that the holographic superfluid is strongly coupled, and that the effects of thermal damping are incorporated. Indeed, the persistent oscillations of the integrable BCS Hamiltonian are replaced here by an under-damped approach towards $|\langle \mathcal{O} \rangle_f| \neq 0$, whilst the power-law damped BCS oscillations are replaced by an exponentially damped approach. The transition at δ_* provides a finite temperature and collision dominated analogue of the collisionless Landau damping transition [16].

Emergent Temperature Scale.— We can gain further insight by considering the phase diagram as a function of the final temperature, T_f , corresponding to the equilibrium temperature of the final state black hole. In

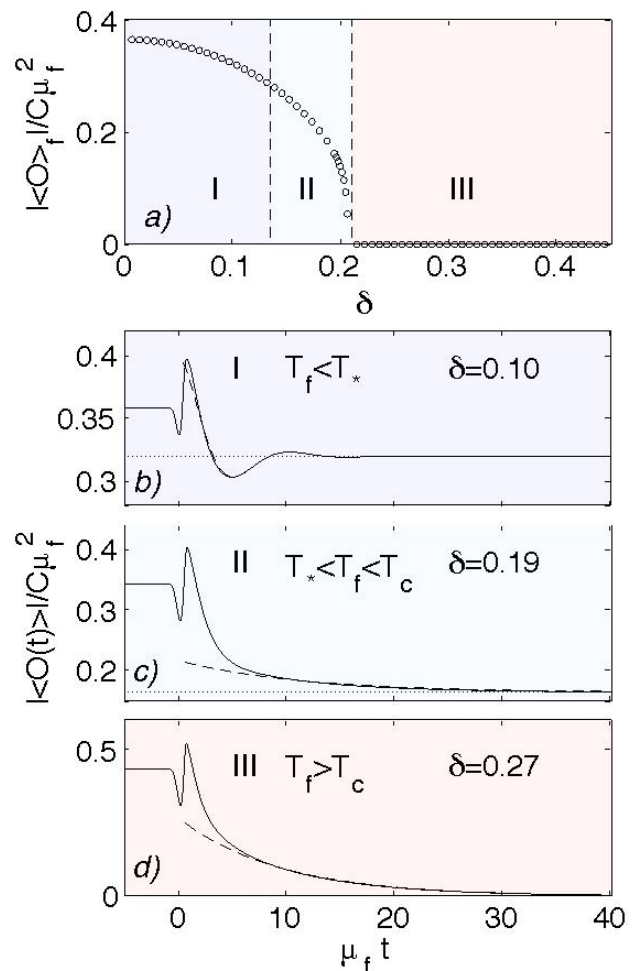


FIG. 2. (a) Dynamical phase diagram of the holographic superfluid showing the final order parameter, $|\langle \mathcal{O} \rangle_f|$, at late times. We start in the superfluid state with $T_i = 0.5T_c$, and monitor the time evolution with increasing quench strength δ . The dynamics exhibits three regimes of behaviour; for the chosen parameters the transitions between these regimes occur at $\delta_* \approx 0.14$ and $\delta_c \approx 0.21$. (b) In region I we observe damped oscillations towards $|\langle \mathcal{O} \rangle_f| \neq 0$. (c) In region II we find a non-oscillatory approach towards $|\langle \mathcal{O} \rangle_f| \neq 0$. (d) In region III we find a non-oscillatory decay towards $|\langle \mathcal{O} \rangle_f| = 0$. The dashed lines in (b), (c), and (d) correspond to the dominant quasi-normal modes of the final state black holes for temperatures $T_f/T_c = 0.73, 0.95, 1.48$ respectively.

Fig. 3(a) we plot T_f versus δ , showing that stronger quenches lead to greater final temperatures, consistent with the notion that the quench leads to heating. Using this relationship we may re-plot the data in Fig. 2 as a function of T_f ; see Fig. 3(b). The data collapse on to the equilibrium phase diagram of the holographic superfluid [35], as indicated by the solid line. The transition from II to III is associated with increasing T_f above T_c . However, Fig. 3(b) contains more information than the equilibrium phase diagram; there is an emergent dynamical temperature scale T_* , associated with δ_* , where the time

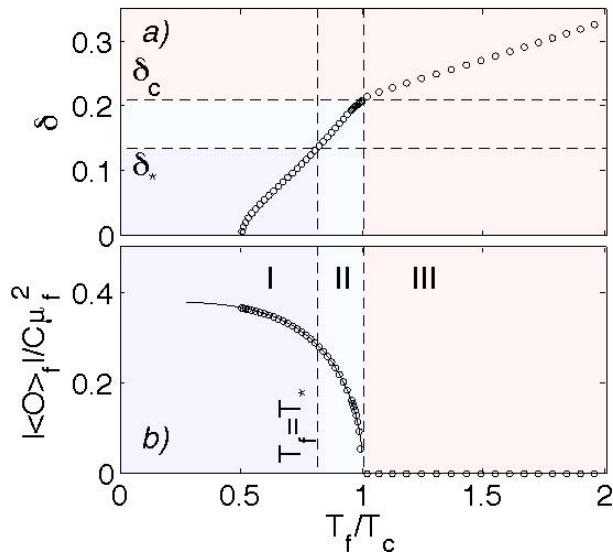


FIG. 3. (a) Final state temperature T_f versus the quench strength δ . We use the same initial parameters as in Fig. 2. (b) Using the relationship in (a) the dynamical boundary in Fig. (2) collapses on to the equilibrium phase diagram of the superfluid [34, 35] as shown by the solid line. The dynamical transition at $\delta_* \approx 0.14$ in Fig. 2 occurs within the superfluid phase at a temperature $T_* \approx 0.81T_c$.

evolution changes from under-damped to over-damped.

Quasi-Normal Modes.— In order to gain insight into the three regimes of collective dynamics, the temperature scale T_* , and to expose its broader relevance, we turn our attention to the late time asymptotics in Figs 2-3. As $t \rightarrow \infty$, the dynamics is described by the quasi-normal modes (QNMs) of the late time black holes. Each QNM describes an approach to equilibrium in linear perturbation theory with time dependence $e^{-i\omega t}$. Those that dominate the late time dynamics have complex frequency ω with the greatest imaginary part and give rise to the behaviour in Eq. (7). As outlined in the Supplementary Material, we have calculated the homogeneous isotropic QNMs both for the AdS-RN black holes (3), and for the superfluid black holes of Ref. [35]. The trajectories of the dominant QNMs in the complex ω plane are depicted in Fig. 4.

Typically, the real parts of the dominant QNM frequencies correspond to oscillations, and the imaginary parts to damping. However, as shown in Fig. 4(c), for temperatures above T_c , the QNMs for the AdS-RN black hole have two complex frequencies that are closest to the real axis. Nonetheless, substitution into Eq. (7) with $\langle \mathcal{O}_f \rangle = 0$ yields the damped non-oscillatory behaviour found in region III of Fig. 2. As the temperature is lowered, these dominant poles migrate upwards in the complex ω plane and at the superfluid transition temperature, T_c , they coincide at $\omega = 0$. This corresponds to the onset of spontaneous U(1) symmetry breaking with the

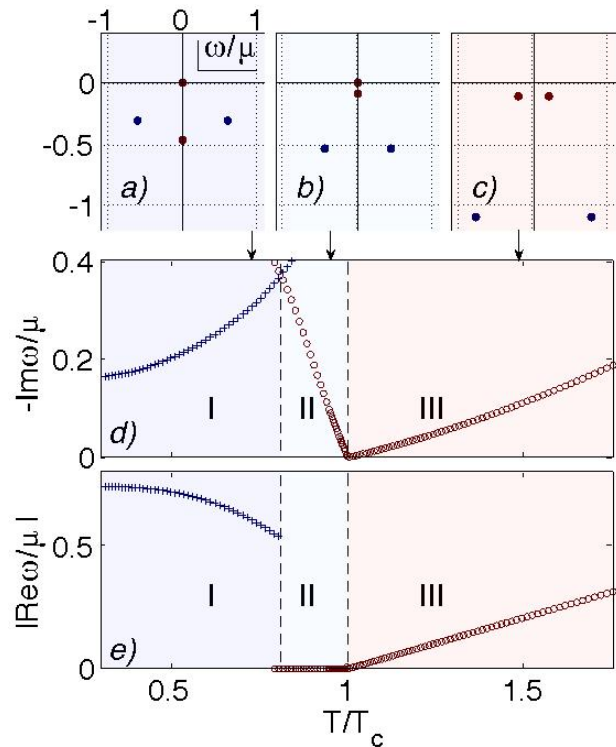


FIG. 4. Evolution of the QNM frequencies with temperature. (a) $T = 0.71T_c$. (b) $T = 0.95T_c$. (c) $T = 1.68T_c$. Time reversal invariance corresponds to $\omega \rightarrow -\omega^*$. (d) and (e) show the imaginary and real parts of the dominant QNMs. i.e. the QNMs closest to the real axis. The results show three regimes of dynamics, in quantitative agreement with Fig. 2.

appearance of a Goldstone mode. Below T_c , one of these modes, the “amplitude” mode, travels down the imaginary axis, consistent with time-reversal invariance under $\omega \rightarrow -\omega^*$, whilst the Goldstone “phase” mode remains pinned at $\omega = 0$; see Fig. 4(b). The amplitude mode describes the damped approach to a finite order parameter as shown in region II of Fig. 2; the Goldstone mode does not affect the dynamics in the homogeneous and isotropic context, although it does lead to a hydrodynamic mode at non-zero spatial momentum. As the temperature is lowered, the subdominant poles also ascend in the complex plane. The dynamical transition temperature T_* corresponds to the temperature at which the damping rate of the descending amplitude mode coincides with that of the ascending subdominant complex poles. For the chosen parameters this occurs at $T_* \approx 0.81T_c$, in agreement with the nonlinear analysis. For temperatures below T_* , the previously subdominant poles now become dominant, as shown in Fig. 4(a). The dynamics corresponds to a damped oscillatory approach to a finite order parameter as found in region I. In addition to this change in dynamics at T_* , one may also extract the variation of the emergent timescales as a function of temperature. As shown in Figs. 4(d) and (e), there are three regimes. Moreover,

the extracted timescales are in quantitative agreement with the late time behaviour of the nonlinear analysis, as indicated by the dashed lines in Figs. 2(b)-(d). It is readily seen that the linear response analysis provides an excellent description over a broad time interval.

Dynamics of Symmetry Breaking.— We now argue that the main results on the late time behaviour of the quenched holographic superfluids, captured in Figs. 2-4, have a surprisingly universal applicability. To see this we first recall, using the holographic dictionary, that the location of the QNMs of the black holes, presented in Fig. 4, correspond to the location of poles of the retarded Green's function for the operator \mathcal{O} in the dual theory [38]. That is, the results can be reformulated in terms of the dual CFT itself, without reference to black hole solutions. Thus, the late time behaviour of the system is governed by the poles of the retarded Green's function that are closest to the real axis, exactly as we have argued above. In particular, the appearance of the scale T_* and the three types of behaviour, labelled I, II and III in Figs. 2 and 3, are a consequence of the pole structure presented in Fig. 4. Now the key point is that the pole structure in Fig. 4 is the *generic* behaviour one expects for an arbitrary homogeneous and isotropic system with time-reversal invariance under $\omega \rightarrow -\omega^*$, which can spontaneously break a continuous global symmetry including the presence of the Goldstone mode at the origin. The precise value of T_* will, of course, depend on the details of the system, but it will always be given by the temperature at which the value of $\text{Im}(\omega)$ for the pole on the imaginary axis, and those poles off the imaginary axis and closest to the real axis, coincide. In general we will have $0 < T_* < T_c$ and hence all three regions I, II and III; for some systems it may be that $T_* = 0$ and hence region I would be absent. For a local symmetry we expect the same phenomenology; the Goldstone mode is replaced by the longitudinal mode of the massive vector which, together with the amplitude mode, will be constrained to be on the lower imaginary axis. It may be possible to compute the pole structure in other models; see for example [39] for a recent calculation of the spectral properties of the $O(N)$ model at zero temperature. Finally, it would be very interesting to experimentally observe the behaviour we are predicting in, for example, a system of cold atoms.

Acknowledgments.— We thank P. Chesler, S. Hartnoll, P. Figueras, L. Lehner, R. Myers, S. Sachdev, K. Schalm and D. Tong for valuable discussions. MJB and BDS acknowledge EPSRC grant EP/E018130/1. JPG acknowledges a Royal Society Wolfson Award. We thank GGI, KITP, Leiden and PI for hospitality and acknowledge NSF grant PHY05-51164.

-
- [1] T. Kinoshita, T. Wenger, and D. S. Weiss, *Nature* **440**, 900 (2006).
 - [2] L. E. Sadler, J. M. Higbie, S. R. Leslie, M. Vengalattore, and D. M. Stamper-Kurn, *Nature* **443**, 312 (2006).
 - [3] R. P. Smith, S. Beattie, S. Moulder, R. L. D. Campbell, and Z. Hadzibabic, [arXiv:1112.4457](https://arxiv.org/abs/1112.4457).
 - [4] M. Endres, T. Fukuhara, D. Pekker, M. Cheneau, P. Schauß, C. Gross, E. Demler, S. Kuhr, and I. Bloch, [arXiv:1204.5183](https://arxiv.org/abs/1204.5183).
 - [5] B. Mansart, J. Lorenzana, M. Scarongella, M. Chergui, and F. Carbone, [arXiv:1112.0737](https://arxiv.org/abs/1112.0737).
 - [6] P. Calabrese and J. Cardy, *Phys. Rev. Lett.* **96**, 136801 (2006).
 - [7] G. Vidal, *Phys. Rev. Lett.* **91**, 147902 (2003).
 - [8] S. R. White and A. E. Feiguin, *Phys. Rev. Lett.* **93**, 076401 (2004).
 - [9] A. J. Daley, C. Kollath, U. Schollwöck, and G. Vidal, *J. Stat. Mech.*, P04005 (2004).
 - [10] A. Polkovnikov, K. Sengupta, A. Silva, and M. Vengalattore, *Rev. Mod. Phys.* **83**, 863 (2011).
 - [11] R. A. Barankov, L. S. Levitov, and B. Z. Spivak, *Phys. Rev. Lett.* **93**, 160401 (2004).
 - [12] E. A. Yuzbashyan, O. Tsyplatyev, and B. L. Altshuler, *Phys. Rev. Lett.* **96**, 097005 (2006).
 - [13] E. A. Yuzbashyan, B. L. Altshuler, V. B. Kuznetsov, and V. Z. Enolskii, *J. Phys. A* **38**, 7831 (2005).
 - [14] R. A. Barankov and L. S. Levitov, *Phys. Rev. Lett.* **93**, 130403 (2004).
 - [15] A. V. Andreev, V. Gurarie, and L. Radzihovsky, *Phys. Rev. Lett.* **93**, 130402 (2004).
 - [16] R. A. Barankov and L. S. Levitov, *Phys. Rev. Lett.* **96**, 230403 (2006).
 - [17] A. F. Volkov and Sh. M. Kogan, *Sov. Phys. JETP* **38**, 1018 (1974).
 - [18] V. Gurarie, *Phys. Rev. Lett.* **103**, 075301 (2009).
 - [19] J. M. Maldacena, *Adv. Theor. Math. Phys.* **2**, 231 (1998).
 - [20] S. S. Gubser, I. R. Klebanov, and A. M. Polyakov, *Phys. Lett. B* **428**, 105 (1998).
 - [21] E. Witten, *Adv. Theor. Math. Phys.* **2**, 253 (1998).
 - [22] U. H. Danielsson, E. Keski-Vakkuri, and M. Kruczenski, *Nucl. Phys. B* **563**, 279 (1999).
 - [23] S. B. Giddings and S. F. Ross, *Phys. Rev. D* **61**, 024036 (2000).
 - [24] S. Bhattacharyya and S. Minwalla, *JHEP* **0909**, 034 (2009).
 - [25] S. R. Das, T. Nishioka, and T. Takayanagi, *JHEP* **1007**, 071 (2010).
 - [26] T. Albash and C. V. Johnson, *New J. Phys.* **13**, 045017 (2011).
 - [27] J. Sonner and A. G. Green, [arXiv:1203.4908](https://arxiv.org/abs/1203.4908).
 - [28] P. M. Chesler and L. G. Yaffe, *Phys. Rev. Lett.* **102**, 211601 (2009).
 - [29] K. Murata, S. Kinoshita, and N. Tanahashi, *JHEP* **1007**, 050 (2010).
 - [30] P. Bizon and A. Rostworowski, *Phys. Rev. Lett.* **107**, 031102 (2011).
 - [31] D. Garfinkle and L. A. Pando Zayas, *Phys. Rev. D* **84**, 066006 (2011).
 - [32] H. Bantilan, F. Pretorius, and S. S. Gubser, *Phys. Rev. D* **85**, 084038 (2012).
 - [33] A. Buchel, L. Lehner, and R. C. Myers, [arXiv:1206.6785](https://arxiv.org/abs/1206.6785).

- [34] S. S. Gubser, Phys. Rev. D **78**, 065034 (2008).
- [35] S. A. Hartnoll, C. P. Herzog, and G. T. Horowitz, Phys. Rev. Lett. **101**, 031601 (2008).
- [36] S. A. Hartnoll, Class. Quant. Grav. **26**, 224002 (2009).
- [37] J. McGreevy, Adv. High Energy Phys. , 723105 (2010).
- [38] E. Berti, V. Cardoso, and A. O. Starinets, Class. Quant. Grav. **26**, 163001 (2009).
- [39] D. Podolsky and S. Sachdev, arXiv:1205.2700.

SUPPLEMENTARY MATERIAL

Nonlinear Dynamics.—To study the response to the quench given in Eq. (6) we solve the equations of motion for Eq. (1) numerically, using the metric described near (2) (see also [29]). The asymptotic boundary is located at $z = 0$ and writing $\psi(t, z) = z[\psi_1(t) + \tilde{\psi}(t, z)]$, $a(t, z) = \mu(t) + \tilde{a}(t, z)$, $F(t, z) = 1 + z^2[-|\psi_1|^2/2 + \tilde{F}(t, z)]$ and $S(t, z) = 1 + z^2[-|\psi_1|^2/4 + \tilde{S}(t, z)]$ we can choose a gauge where $\tilde{\psi} \sim \psi_2(t)z$, $\tilde{a} \sim \rho(t)z$, and \tilde{F}, \tilde{S} also vanish linearly as $z \rightarrow 0$. Notice that the residual coordinate freedom $1/z \rightarrow 1/z + f(t)$ is fixed by these asymptotics. In contrast to [29], we adopt a gauge for μ so that $\text{Im}(\psi_2 - D\psi_1) = 0$, where $D = \partial_t - 2i\mu$. One can show that the equations imply the boundary charge conservation equation, given by $\dot{\rho} = -4\text{Im}[\psi_1^*(\psi_2 - D\psi_1)]$, and also a (sourced) energy conservation equation. Our choice of quench, with ψ_1 real as in Eq. (6), ensures that the initial and final charge densities are the same. Specifically, this can be seen by considering Eq (5) and observing that we have $\dot{\rho} = 0$ and also $\dot{\mu} = 0$ at $t = \pm\infty$. With S, F, A_t and the complex scalar ψ we have 5 real quantities to evolve as functions of the coordinates t, z . There are 8 (real) equations of motion from the metric, vector and scalar equations, 5 of which we use as evolution equations for the variables $\tilde{\psi}, \tilde{a}, \tilde{F}, \tilde{S}$, and the remaining 3 are constraints. The 5 equations have principal parts, $\partial_{t^2}^2 \psi - \frac{1}{2}F\partial_z^2 \tilde{\psi} = 0$, $\partial_{t^2}^2 \tilde{a} = 0$, $\partial_{t^2}^2 \tilde{S} = 0$, and $F\partial_z^2 \tilde{S} + S\partial_z^2 \tilde{F} = 0$, where the latter is elliptic. Provided the initial data satisfies the 3 constraints then two of them, with principal parts $\partial_z^2 \tilde{S} = 0$ and $\partial_z^2 \tilde{a} = 0$, are automatically satisfied at later times. The one remaining constraint, with principal part $\partial_t^2 \tilde{S} = 0$, must be imposed at the boundary in addition to the 5 equations of motion in the bulk. Physically, this corresponds to (sourced) boundary stress energy conservation, and provides the additional data required for the elliptic evolution equation. Note that (sourced) current conservation results from the evolution equations and is not imposed separately.

To solve the equations of motion numerically we use a Chebyshev pseudo spectral representation in $z \in [0, 1]$, where the initial horizon is located at $z = 1$, and use an implicit Crank-Nicholson finite difference scheme in t . Given a slice at constant t we advance to the next slice by solving for $\tilde{\psi}, \tilde{a}, \tilde{F}, \tilde{S}$ from the 5 evolution equations together with the boundary constraint and gauge condition for μ ; note that we are not required to impose any boundary condition at the innermost point $z = 1$ since this is inside the event horizon. The method outlined above is very robust, and by virtue of the spectral representation in z it allows very accurate extraction of boundary quantities. We find that relatively modest grid sizes with 20 points in z already give reliable results. The data presented in this paper is for 40 points, where convergence testing indicates that the errors will be less than percent level in all the plotted quantities. We construct static superfluid black hole solutions of [35] for the initial data by solving the usual ordinary differential equation shooting problem in our gauge. We then find that we can stably evolve up to times $t \sim 60 \mu_i^{-1}$, to extract the data presented here. If one runs for too long then we sometimes encounter the black hole singularity. In order to evolve further one must implement singularity excision which we leave for future work. Our present results are in full quantitative agreement with the QNM analysis described in the text and below.

Quasi-Normal Modes (QNMs).— The QNMs of the equilibrium black holes of Eq. (1) are linearised perturbations with ingoing boundary conditions at the black hole horizon and normalisable boundary conditions at the asymptotic AdS boundary; for a review see Ref. [38]. For the purposes of this paper we only consider the zero momentum sector of the QNM spectra. Furthermore, to determine the late dynamics of the charged scalar field, ψ , we only analyse the sector involving ψ . For the AdS-RN black hole (3) we find a second order ODE for ψ . For the superfluid black hole of [35] which has $\psi \neq 0$, we can use the gauge freedom, arising from diffeomorphisms and local U(1) transformations of the background, to reduce the problem to two second order ODEs for two gauge invariant variables involving ψ, A and the metric. In both cases we then use Chebyshev pseudo-spectral differencing to cast the linear perturbation equations into the form, $M(\omega; \lambda)\mathbf{v} = 0$. The matrix M depends on the complex frequency ω and the background parameters λ , such as the temperature and chemical potential. The vector \mathbf{v} consists of the two gauge-invariant variables evaluated at the grid points. The QNM frequencies are then determined by the condition $|M(\omega; \lambda)| = 0$.